

Supporting Information

Red-to-blue paper-based colorimetric sensor integrated with smartphone for point-of-use analysis of cerebral AChE upon Cd²⁺ exposure

Chang Liu^{a,b}, Yuxin Luo^{a,b}, Huijie Wen^{a,b}, Yanxia Qi^c, Guoyue Shi^c, Jingjing Deng^{*a,b},
Tianshu Zhou^{a,b}

^aSchool of Ecological and Environmental Sciences, Shanghai Key Lab for Urban Ecological Process and Eco-Restoration, East China Normal University, 500 Dongchuan Road, Shanghai 200241, China.

^bInstitute of Eco-Chongming, 3663 Zhongshan Road, Shanghai 200062, China.

^cSchool of Chemistry and Molecular Engineering, East China Normal University, 500 Dongchuan Road, Shanghai 200241, China.

* Corresponding Author: E-mail: jjdeng@des.ecnu.edu.cn

Fax: +86-21-54341113, Tel: +86-21-54341113

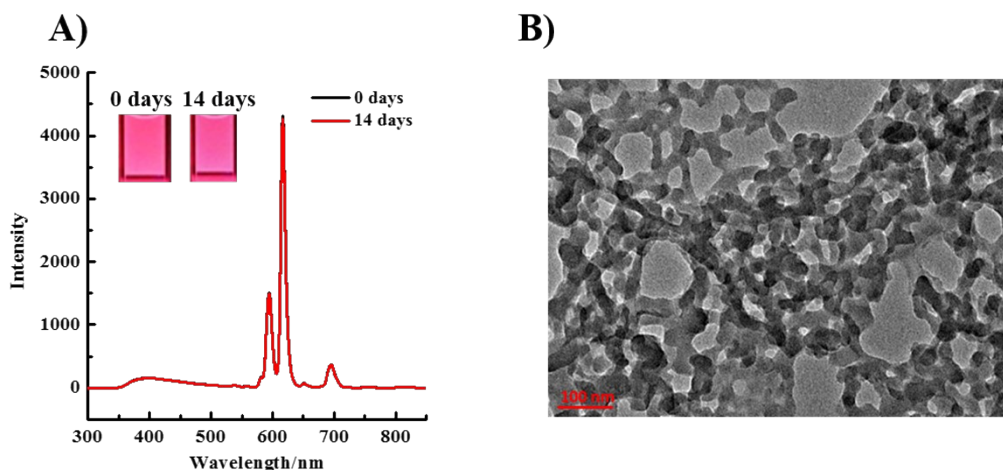


Fig. S1. (A) Fluorescent emission spectra and photographs (Inset) and (B) TEM image of the CDs@Eu/GMP ICP nanoparticles after 14 days.

As shown in Fig. S1A, even after 14 days, both the fluorescence color and the fluorescent intensity of CDs@Eu/GMP ICP nanoparticles all remained unchanged. Furthermore, TEM image of spherical network structure for CDs@Eu/GMP ICP nanoparticles after 14 days storage (Fig. S1B), was also indicative of the good stability of the as-formed CDs@Eu/GMP ICP nanoparticles. The results demonstrated in our study suggested that the CDs@Eu/GMP ICP nanoparticles with long time storage feature is of great potential to develop paper-based colorimetric sensors.

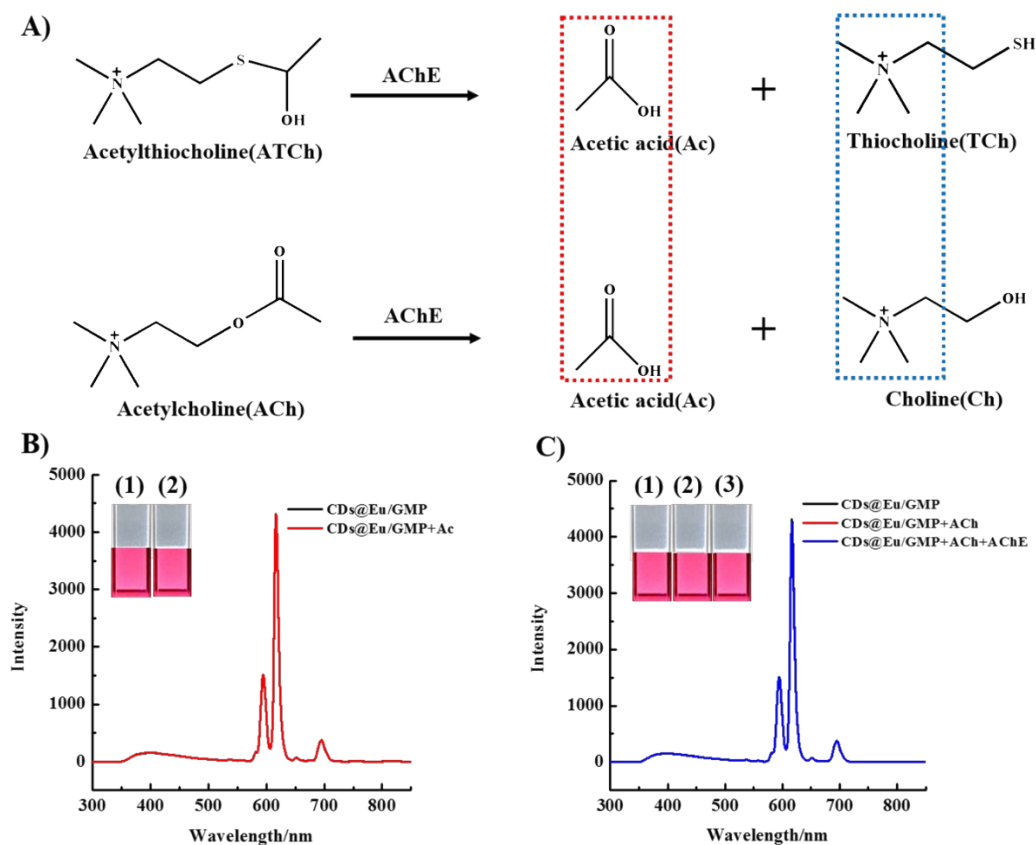


Fig. S2. (A) Schematic illustration for the hydrolysis process of acetylthiocholine (ATCh) (upper) and acetylcholine (ACh) (lower); (B) Fluorescence emission spectra and photographs (Inset) of CDs@Eu/GMP ICP nanoparticles without (vial 1) and with acetic acid (0.8 mM) (vial 2); (C) Fluorescence emission spectra and photographs (Inset) of CDs@Eu/GMP ICP nanoparticles (vial 1), CDs@Eu/GMP ICP nanoparticles in the presence of ACh (0.8 mM) (vial 2), CDs@Eu/GMP ICP nanoparticles in the presence of ACh (0.8 mM) and AChE (10 mU mL⁻¹) (vial 3).

In order to further verify the chemical interaction between the enzymatic products (Fig. S2A, upper, thiocholine (TCh) and acetic acid (Ac)) and CDs@Eu/GMP ICP nanoparticles, Ac (0.8 mM) (red dotted frame) was firstly added to the dispersion of CDs@Eu/GMP ICP nanoparticles. As displayed in Fig. S2B, with the presence of Ac, nearly no change could be noticed either from the white colloid or the fluorescence of CDs@Eu/GMP ICP nanoparticles, indicating that the production of Ac during the enzymatic reaction did not

result in any effect on CDs@Eu/GMP ICP nanoparticles. Therefore, it is speculated that TCh, the other enzyme product, plays a key role in the structural alteration of CDs@Eu/GMP ICP nanoparticles. As depicted in Fig. S2A (upper), there are mainly two functional groups in TCh, both quaternary ammonium group and thiol group may possibly interfere the coordination environment of CDs@Eu/GMP ICP nanoparticles. To figure out the specific functional group more clearly, the substrate acetylthiocholine (ATCh) was replaced by acetylcholine (ACh), to give birth to choline (Ch) with quaternary ammonium groups (blue dotted frame) but without thiol group (Fig. S2A, lower). As can be seen clearly from Fig. S2C, not only the sole addition of ACh, but also the addition of AChE treated ACh did not result in any response of CDs@Eu/GMP ICP nanoparticles: the white colloid of CDs@Eu/GMP ICP nanoparticles with red fluorescence remained unchanged (Fig. S2C, inset), suggesting that Ch with quaternary ammonium groups (blue dotted frame) while without thiol group would not lead to the structural changes of CDs@Eu/GMP ICP nanoparticles. This result also confirmed that the thiol group rather than ammonium group in TCh may interact with CDs@Eu/GMP ICP nanoparticles and eventually result in their structural changes.

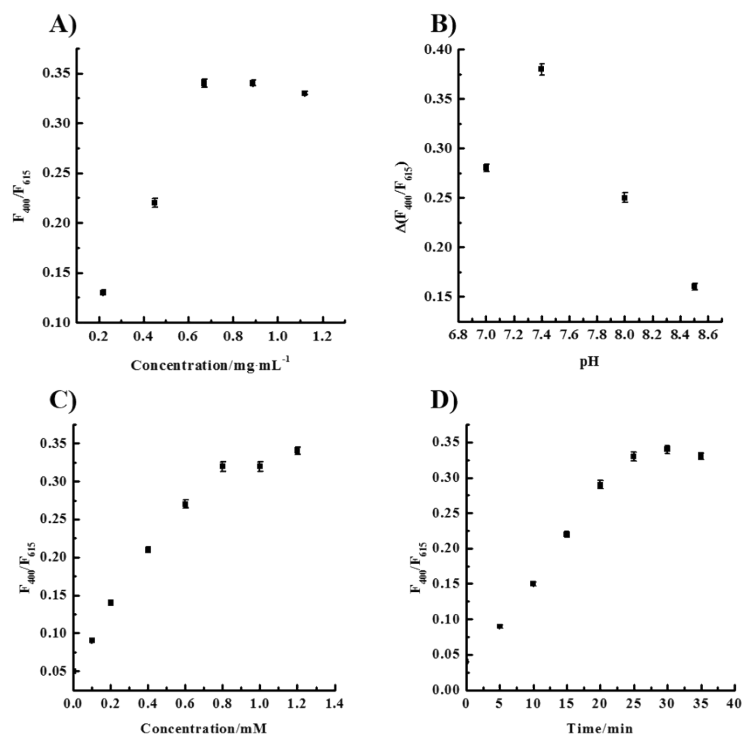


Fig. S3. (A) The effects of different concentration of CDs@Eu/GMP ICP nanoparticles (0.22 mg mL^{-1} , 0.45 mg mL^{-1} , 0.67 mg mL^{-1} , 0.89 mg mL^{-1} , 1.12 mg mL^{-1}); (B) Different pH in the presence of 30 mU mL^{-1} AChE (7, 7.4, 8, 8.5); (C) Different concentration of ATCh (0 mM, 0.1 mM, 0.2 mM, 0.4 mM, 0.6 mM, 0.8 mM, 1 mM, 1.2 mM); (D) Reaction time between AChE (30 mU mL^{-1}) and ATCh (0.8 mM) (0 min, 5 min, 10 min, 15 min, 20 min, 25 min, 30 min, 35 min).

According to previous studies, the activity of AChE depends largely on CDs@Eu/GMP ICP nanoparticles concentration, pH value, ATCh concentration and reaction time.¹ Here, the concentration of CDs@Eu/GMP ICP nanoparticles was firstly optimized. As shown in the Fig. S3A, when the concentration of CDs@Eu/GMP ICP nanoparticles was higher than 0.67 mg mL^{-1} , the ratio of F_{400}/F_{615} remained almost unchanged, while excessive ICP nanoparticles could not be disrupted in the presence of AChE treated ATCh, the concentration of CDs@Eu/GMP ICP nanoparticles was determined to be 0.67 mg mL^{-1} . The influence of pH value was next investigated. As depicted in Fig. S3B, when the pH value

was settled at physiological pH 7.4, AChE was highly activated, this result also validated the further exploration of the CDs@Eu/GMP ICP nanoparticles for AChE activity detection in rat brain. Moreover, as depicted in Fig. S3C, when the concentration of ATCh was higher than 0.8 mM, the ratio of F_{400}/F_{615} of CDs@Eu/GMP ICP nanoparticles reached maximum and was almost unchanged, while high concentration of ATCh may cause a negative impact on the sensitive detection of enzyme activity, the concentration of ATCh was rationally optimized at 0.8 mM. In addition, as shown in the Fig. S3D, the ratio of F_{400}/F_{615} increased gradually with the increasing of reaction time to 30 min, indicating the completion of enzymatic reaction, thereby 30 min was chosen as the appropriate reaction time.

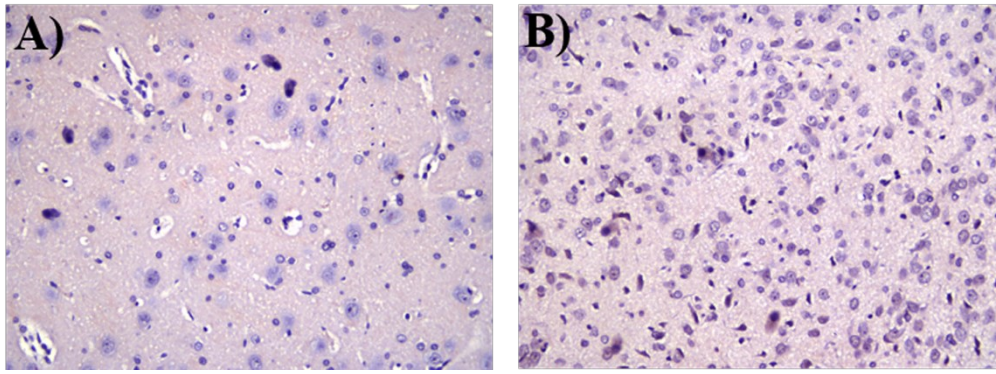


Fig. S4. (A) Images of prefrontal cortex immunostained with congo red from normal rats within 90 days; (B) Images of prefrontal cortex immunostained with congo red from CdCl₂-exposed rats within 90 days.

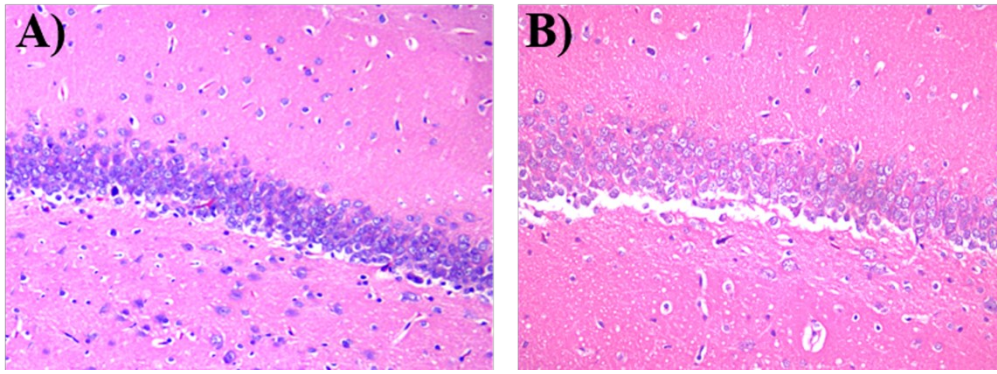


Fig. S5. (A) Images of hippocampal vertebral cells immunostained with hematoxylin-eosin from normal rats within 90 days; (B) Images of hippocampal vertebral cells immunostained with hematoxylin-eosin from CdCl₂-exposed rats within 90 days.

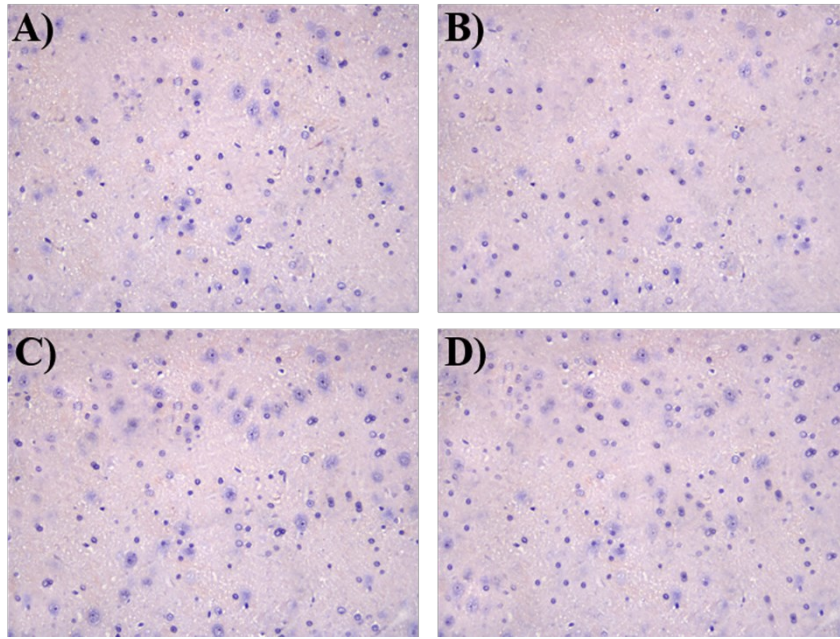


Fig. S6. Images of prefrontal cortex immunostained with congo red from normal rats within 30 days (A) and 60 days (C); Images of prefrontal cortex immunostained with congo red from CdCl₂-exposed rats within 30 days (B) and 60 days (D).

The images of congo red immunostained prefrontal cortex were displayed in Fig. S6. As shown in Fig. S6A and C, no obvious amyloid plaque was observed in the prefrontal cortex of normal rats within 60 days. Also, within 60 days, there was no obvious amyloid plaque in the prefrontal cortex of rats exposed to Cd²⁺ (Fig. S6B and Fig. S6D).

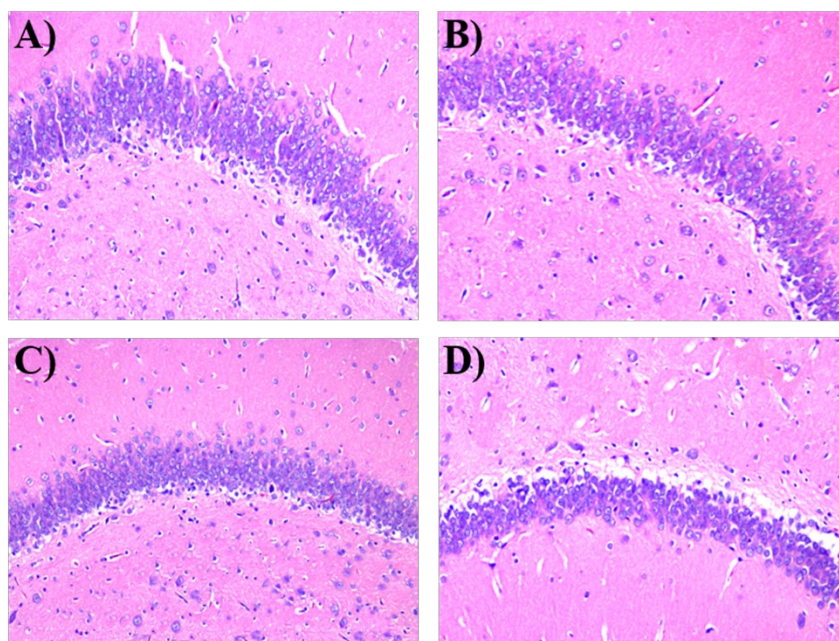


Fig. S7. Images of hippocampal vertebral cells immunostained with hematoxylin-eosin from normal rats within 30 days (A) and 60 days (C); Images of hippocampal vertebral cells immunostained with hematoxylin-eosin from CdCl₂-exposed rats within 30 days (B) and 60 days (D).

The images of hematoxylin-eosin immunostained hippocampal vertebral cells were shown in Fig. S7. As displayed in Fig. S7A and C, for normal rats, the hippocampal vertebral cells within 60 days were closely and tightly arranged. Similarly, for Cd²⁺-exposed rats, the hippocampal vertebral cells in rats exposed to Cd²⁺ within 60 days exhibited regular and tight arrangement (Fig. S7B and Fig. S7D).

Table S1. The comparison of fluorescent methods for the detection of AChE.

Methods	Sensor	Enzyme	Detection limit (mU mL ⁻¹)	Real samples	Refs.
Colorimetry and Fluorescence	RB-AuNP	AChE	1 (C), 0.1 (F)	Cerebrospinal fluid	2
Fluorescence	DNA-Cu/AgNCs	AChE	0.05	None	3
Fluorescence	Carbon quantum dots	AChE	4.25	Human serum and seminal plasma	4
Fluorescence	PSA-carbon quantum dots	AChE	2.6	None	5
Fluorescence	GQDs-MnO ₂	AChE	0.37	Cerebrospinal fluid	6
Fluorescence	Black phosphorus quantum dots	AChE	0.04	None	7
Fluorescence	Carbon dots	AChE	0.1	Human whole blood	8
Fluorescence	CDs@Eu/GMP ICP nanoparticles	AChE	0.033	Cerebrospinal fluid and brain tissues	This work

Table S2. The concentration of AChE in hippocampus from normal rats and CdCl₂-exposed rats was calculated using the calibration curve of the B/R ratio from the photographs of paper-based sensor and the fluorescence spectra.

The concentration of AChE (mU mL⁻¹)			
Exposure time	Group	Based paper-based sensor calibration curve	Based optical spectra calibration curve
30 days	Normal	455.7 ± 1.5	452.5 ± 0.3
	CdCl₂	395.0 ± 7.0	397.8 ± 0.3
60 days	Normal	437.3 ± 2.1	441.0 ± 0.7
	CdCl₂	361.3 ± 2.5	363.7 ± 0.6
90 days	Normal	439.3 ± 5.9	437.0 ± 1.2
	CdCl₂	328.0 ± 5.4	325.0 ± 1.4

Table S3. The concentration of AChE in prefrontal cortex from normal rats and CdCl₂-exposed rats was calculated using the calibration curve of the B/R ratio from the photographs of paper-based sensor and the fluorescence spectra.

The concentration of AChE (mU mL⁻¹)			
Exposure time	Group	Based paper-based sensor calibration curve	Based optical spectra calibration curve
30 days	Normal	522.3 ± 3.2	523.3 ± 0.7
	CdCl₂	449.7 ± 4.0	451.5 ± 0.9
60 days	Normal	525.7 ± 1.6	525.3 ± 0.3
	CdCl₂	397.7 ± 3.8	398.3 ± 0.8
90 days	Normal	519.7 ± 3.5	514.0 ± 0.7
	CdCl₂	333.0 ± 2.0	333.0 ± 0.7

Table S4. The concentration of AChE in striatum from normal rats and CdCl₂-exposed rats was calculated using the calibration curve of the B/R ratio from the photographs of paper-based sensor and the fluorescence spectra.

The concentration of AChE (mU mL⁻¹)			
Exposure time	Group	Based paper-based sensor calibration curve	Based optical spectra calibration curve
30 days	Normal	351.3 ± 5.5	352.8 ± 0.5
	CdCl₂	316.0 ± 6.9	311.8 ± 0.2
60 days	Normal	343.0 ± 6.6	348.3 ± 0.6
	CdCl₂	285.7 ± 3.8	288.7 ± 2.0
90 days	Normal	346.3 ± 2.5	345.0 ± 0.7
	CdCl₂	269.7 ± 4.6	265.0 ± 0.7

Table S5. Effect of Cd²⁺ on MDA content ($\mu\text{mol g}^{-1}$) in rat brains (mean \pm SD, n=4)

Brain regions	Normal (30 days)	CdCl₂* (30 days)	Normal (60 days)	CdCl₂* (60 days)	Normal (90 days)	CdCl₂* (90 days)
Hippocampus	2.17 \pm 0.07	3.81 \pm 0.05	2.18 \pm 0.07	4.37 \pm 0.04	2.18 \pm 0.08	5.55 \pm 0.06
Prefrontal cortex	1.71 \pm 0.05	3.56 \pm 0.04	1.73 \pm 0.05	3.84 \pm 0.05	1.74 \pm 0.03	4.99 \pm 0.07
Striatum	1.05 \pm 0.05	2.33 \pm 0.03	1.03 \pm 0.03	2.63 \pm 0.04	1.05 \pm 0.06	3.83 \pm 0.07

*P < 0.0001 compared with normal group.

Table S6. Effect of Cd²⁺ on CAT activity (U mg⁻¹) in rat brains (mean ± SD, n=4)

Brain regions	Normal (30 days)	CdCl₂* (30 days)	Normal (60 days)	CdCl₂* (60 days)	Normal (90 days)	CdCl₂* (90 days)
Hippocampus	4.01 ± 0.05	3.52 ± 0.04	4.01 ± 0.02	3.32 ± 0.04	4.00 ± 0.04	3.15 ± 0.04
Prefrontal cortex	4.20 ± 0.02	3.61 ± 0.04	4.16 ± 0.06	3.43 ± 0.02	4.16 ± 0.08	3.20 ± 0.02
Striatum	4.03 ± 0.02	3.58 ± 0.02	4.01 ± 0.02	3.46 ± 0.04	4.03 ± 0.03	3.18 ± 0.02

*P < 0.0001 compared with normal group.

Table S7. Effect of Cd²⁺ on SOD activity (U mg⁻¹) in rat brains (mean ± SD, n=4)

Brain regions	Normal (30 days)	CdCl₂* (30 days)	Normal (60 days)	CdCl₂* (60 days)	Normal (90 days)	CdCl₂* (90 days)
Hippocampus	1.31 ± 0.03	0.91 ± 0.02	1.29 ± 0.03	0.85 ± 0.04	1.24 ± 0.06	0.65 ± 0.02
Prefrontal cortex	0.86 ± 0.02	0.68 ± 0.01	0.88 ± 0.02	0.48 ± 0.01	0.88 ± 0.02	0.34 ± 0.02
Striatum	1.11 ± 0.02	0.84 ± 0.02	1.12 ± 0.03	0.74 ± 0.02	1.11 ± 0.03	0.60 ± 0.01

*P < 0.0001 compared with normal group.

Table S8. The concentration of AChE in CSF from normal rats and CdCl₂-exposed rats was calculated using the calibration curve of the B/R ratio from the photographs of paper-based sensor and the fluorescence spectra.

The concentration of AChE (mU mL⁻¹)			
Exposure time	Group	Based paper-based sensor calibration curve	Based optical spectra calibration curve
30 days	Normal	573.0 ± 3.6	570.3 ± 0.6
	CdCl₂	495.6 ± 5.0	495.0 ± 0.3
60 days	Normal	563.0 ± 7.2	569.7 ± 0.2
	CdCl₂	429.0 ± 5.3	437.7 ± 0.9
90 days	Normal	553.3 ± 6.0	560.7 ± 1.2
	CdCl₂	361.0 ± 1.6	369.0 ± 0.7

Reference

- 1 R. X. Ma, M. Xu, C. Liu, G. Y. Shi, J. J. Deng and T. S. Zhou, *ACS Appl. Mater. Interfaces*, 2020, **12**, 42119-42128.
- 2 D. B. Liu, W. Chen, Y. Tian, S. He, W. F. Zheng, J. S. Sun, Z. Wang and X. Y. Jiang, *Adv. Healthcare Mater.*, 2012, **1**, 90-95.
- 3 W. H. Li, W. Li, Y. F. Hu, Y. L. Xia, Q. P. Shen, Z. Nie, Y. Huang and S. Z. Yao, *Biosens. Bioelectron.*, 2013, **47**, 345-349.
- 4 Z. S. Qian, L. J. Chai, C. Tang, Y. Y. Huang, J. R. Chen and H. Feng, *Sens. Actuators B: Chem.*, 2016, **222**, 879-886.
- 5 F. Q. Zhou, H. Feng, Y. F. Fang, Q. Sun and Z. S. Qian, *RSC Adv.*, 2016, **6**, 105454-105460.
- 6 J. J. Deng, D. K. Lu, X. L. Zhang, G. S. Shi and T. S. Zhou, *Environ. Pollut.*, 2017, **224**, 436-444.
- 7 W. Gu, Y. H. Yan, X. Y. Pei, C. L. Zhang, C. P. Ding and Y. Z. Xian, *Sens. Actuators B: Chem.*, 2017, **250**, 601-607.
- 8 X. M. Xu, Y. Cen, G. H. Xu, F. D. Wei, M. L. Shi and Q. Hu, *Biosens. Bioelectron.*, 2019, **131**, 232-236.